Since January 2020 Elsevier has created a COVID-19 resource centre with free information in English and Mandarin on the novel coronavirus COVID-19. The COVID-19 resource centre is hosted on Elsevier Connect, the company's public news and information website.

Building and Environment 219 (2022) 109247

Contents lists available at ScienceDirect

Building and Environment

journal homepage: www.elsevier.com/locate/buildenv

Droplet aerosols transportation and deposition for three respiratory behaviors in a typical negative pressure isolation ward

Yongxin Wang [a], Zhijian Liu [a,*], Haiyang Liu [a], Minnan Wu [a], Junzhou He [a], Guoqing Cao [b]

[a] Department of Power Engineering, North China Electric Power University, Baoding, Hebei, 071003, PR China
[b] Institute of Building Environment and Energy, China Academy of Building Research, Beijing, 100013, PR China

ARTICLE INFO

Keywords:
Droplet aerosols
Negative pressure isolation ward
Full-scale experiment
Airflow

ABSTRACT

Negative pressure isolation wards could provide safety for health care workers (HCWs) and patients infected with SARS-CoV-2. However, respiratory behavior releases aerosols containing pathogens, resulting in a potential risk of infection for HCWs. In this study, the spatiotemporal distribution of droplet aerosols in a typical negative pressure isolation ward was investigated using a full-scale experiment. In this experiment, artificial saliva was used to simulate the breathing behavior, which can reflect the effect of evaporation on droplet aerosols. Moreover, numerical simulations were used to compare the transport of droplet aerosols released by the three respiratory behaviors (breathing, speaking, and coughing). The results showed that droplet aerosols generated by coughing and speaking can be removed and deposited more quickly. Because reduction in the suspension proportion per unit time was much higher than that in the case of breathing. Under the air supply inlets, there was significant aerosol deposition on the floor, while the breathing area possessed higher aerosol concentrations. The risk of aerosol resuspension and potential infection increased significantly when HCWs moved frequently to these areas. Finally, more than 20% of the droplet aerosols escaped from the ward when the number of suspended aerosols in the aerosol space was 1%.

1. Introduction

Since 2019, the SARS-CoV-2 virus has spread globally. As of March 2022, the cumulative number of cases reported globally was over 457 million, and the cumulative number of deaths was over 6 million. Vaccination has been widespread in many countries to curb the spread of epidemics. However, because of Omicron's high transmissibility and low severity, vaccines are far less effective than expected [1]. Therefore, the most effective way to control the epidemic is isolation and treatment. As early as the SARS outbreak, the importance of isolation treatment has become a major concern [2]. As the most important infrastructure for the treatment of patients infected with SARS-CoV-2, a negative pressure isolation ward guarantees safety for health care workers (HCWs) [3,4]. From SARS (2003) to COVID-19 (2019), multiple studies have demonstrated that aerosol transportation is an important method of virus diffusion [5–7]. Therefore, it is necessary to study the transportation and deposition of droplet aerosols in the negative pressure isolation ward, which can provide suggestions for ensuring the safety of HCWs.

In recent years, the foci of aerosols transmission were sustained in the negative pressure isolation ward. Jurelionis et al. compared the effects of displacement ventilation and mixed ventilation in a full-scale experiment [8]. The results showed that mixed ventilation could reduce the air age in the ventilation room and increase the pollutant removal efficiency. Yin et al. also compared the effects of displacement ventilation and mixed ventilation on aerosol escape [9]. These findings suggest that displacement ventilation may lead to pollutant accumulation in the upper part of the room. Zhao et al. showed that the average particle concentration in displacement-ventilated rooms was higher than that in mixed-ventilation rooms [10]. In addition, Olmedo et al. reported a higher concentration of contaminants in the case of displacement ventilation [11]. Consequently, mixed ventilation is more efficient for removing aerosols. Therefore, in this study, the transportation and deposition of aerosol droplets were studied by considering only the mixed ventilation mode. However, in the above studies, the differences in the diameter distribution and initial velocity of droplet aerosols released with different respiratory behaviors were ignored. In fact, different breathing behaviours of patients (breathing, speaking, and coughing) have different airflow rates [12–14] and aerosol particle size distributions [13,15–17]. Hence, the transportation and deposition

* Corresponding author.
E-mail address: zhijianliu@ncepu.edu.cn (Z. Liu).

https://doi.org/10.1016/j.buildenv.2022.109247
Received 16 April 2022; Received in revised form 22 May 2022; Accepted 26 May 2022
Available online 30 May 2022

of droplet aerosols released by three different respiratory behaviours in a negative-pressure isolation ward were compared.

Droplet aerosols produced by respiratory behavior (including breathing, speaking, and coughing) can carry various pathogens and are transmitted by airflow. Airborne transmission may be the dominant route for many respiratory infections [18]. In addition, the deposition of the droplet aerosols on surface causes a significantly risk on the fomite transmission [19,20]. In previous studies, many tracer gases, such as SF_6 [9], CO_2 [21], smoke [22], have been used to experimentally study the diffusion of aerosols in rooms. However, experiments using tracer gases have ignored the evaporation of droplet aerosols. Therefore, volatile and non-volatile substances were used to prepare artificial saliva for experiments; for example, diisooctyl sebacate was mixed with isopropanol (C_3H_8O) [23], and 75% distilled water was mixed with 25% pure glycerine [24] to prepare artificial saliva. In fact, mixtures similar to human exhaled droplet aerosols can better simulate droplet aerosol evaporation and transport in real situations. Therefore, in our droplet aerosol experiments, artificial saliva was used as the aerosol-generating material, and its evaporation ratio was close to that of real saliva [25].

Here, the spatial distribution of droplet aerosols and the characteristic of surface deposition were studied in a typical negative pressure isolation ward. In droplet aerosol experiments, artificial saliva with a mass concentration of 8% non-volatile components was used as the aerosol generating material. Breathing, talking, and coughing were the main respiratory behaviors of patients infected with SARS-CoV-2 [26,27]. According to a recent study, 49.8% of Omicron patients suffered from persistent cough [28]. Therefore, we compared the effects of these three respiratory behaviors on the droplet aerosol transport and deposition. In addition, a numerical model was established based on the actual ward to further analyze the transport and deposition of aerosols. The research results would provide suggestions and references for the design and daily operation of negative-pressure isolation wards.

2. Methodology

2.1. Model description and numerical case design

In the negative-pressure isolation ward, the transport and distribution characteristics of droplet aerosols were studied. The pressure gradient was set according to Requirements of environmental control for the hospital negative pressure isolation ward (GB/T 35428–2017), with −15 Pa in the ward, −10 Pa in the buffer room, and −20 Pa in the bathroom. A physical model was constructed using Space Claim 2021R1 software, and a part of the physical model in the room was simplified. The detailed dimensions are listed in Table 1. As shown in Fig. 1(a), two air supply inlets located on the ceiling were used to supply clean air. An exhaust vent was installed at the bottom of the air shaft on the wall side. Door-1 of the room was connected to the buffer room, and Door-2 was connected to the toilet. Two door gaps were installed at the bottom, considering air leakage under actual working conditions. After measuring the velocity, the average airflow velocity at door gap-1 was 2 m/s, while the average airflow velocity at door gap-2 was 2.3 m/s. According to the design principle of the negative-pressure isolation ward, the airflow to the ward exists in the door gap connected to the buffer room. However, the door gap connected to the toilet had airflow outside the ward, as shown in Fig. 1(b).

Table 1
Indoor related parameters.

Name	Number	Size(m) X × Y × Z	Temperature (K)	Boundary condition
Isolation ward	1	4.22 × 2.8 × 2.66	–	–
Model of human	1	0.3 × 0.4 × 1.7	307.1	Trap
Supply inlet	2	0.135 × 0.24	299.1	Reflect
Exhaust vent	1	0.27 × 0.27	–	Escape
Door gap-1 (buffer room)	1	1.14 × 0.02	–	Reflect
Door gap-2 (toilet)	1	0.9 × 0.02	–	Escape
Bed	1	0.9 × 0.5 × 1.94	–	Trap
Wall	–	–	–	Trap
Equipment belt	–	2.34 × 0.06 × 0.02	–	Trap
Table	1	0.45 × 0.75 × 0.42	–	Trap

Fabian et al. used an optical particle counter as well as qPCR techniques to analyze the particle size of the pollutants exhaled by the breath of influenza patients, and approximately 70% of the particles had a diameter of 0.3–0.5 μm, and 20% of the particles had a diameter of 0.5–1 μm [13]. According to our study, considering the effect of evaporation, the diameter of the particles was set to 1 μm, and the average exhalation velocity while breathing was 0.5 m/s. According to the results of a study, the average velocity of the airflow while speaking was set to 3.9 m/s, with a diameter of 13.5 μm, and the average exhalation velocity while coughing was 11.7 m/s, with a diameter of 16.0 μm [15]. According to the experimental conditions, the temperature of the air supply airflow was set to 299.1 K, and the relative humidity was 60%. The relative humidity of the expiratory airflow was 90%, and the temperature was 309.1 K [29]. Chao et al. showed that coughing produces approximately twice as many droplets as speaking does [15]. At the same time, multiple measurements by Morawska et al. indicated that the concentration ratio of droplet aerosols produced by breathing, speaking, and coughing was 1:3:6 [29]. Thus, the aerosol release rates while breathing, speaking, and coughing were set to be 214/s, 642/s, and 1284/s respectively. According to our experimental results, Aerosol concentrations remain relatively stable and the aerosol concentration of the four measuring points did not change significantly with time after the aerosol was released for 600s. Therefore, the droplet aerosol can be designed as 600s in the numerical calculation. Droplet aerosols from a single coughing or speaking were not sufficient to obtain statistical results. Hence, multiple and consecutive coughing and speaking were studied, which was also used in similar studies [23,31]. According to related research [23,30], inhalation has little effect on the spatial distribution of droplet aerosol, so the process of inhalation was ignored.

2.2. Droplet aerosols experiment

To study the transport and spatial distribution of the droplet aerosols generated by respiratory behaviors, aerosol emission experiments were conducted in a typical negative-pressure isolation ward. The layout of the ward environment is shown in Fig. 1(a). The isolation ward consisted of an aerosol generation system, a heating dummy model, four sampling racks, and an optical particle sizer (TSI 3330, particle size resolution of less than 5% at 0.5 μm, and a sampling flow is 1 L/min) with a range of 0.3–10 μm. The heating dummy was formed by winding $Cr_{20}Ni_{80}$ resistance wire (wire diameter 0.9 mm, resistivity 1.13 Ω/m) around the mannequin with a direct-current power source. Temperature sensors (negative temperature coefficient thermistor with a resistance value of 10 K, thermal coefficient of 3950, and sensitivity of 0.1 K) were installed on the upper body, legs, and arms of the mannequin, and the surface temperature of the dummy modal was maintained at 34 ± 1 °C. The configuration of artificial saliva was based on previous studies [25,32]. Phosphate Buffer saline (PBS) was used as the solvent, and pure propanetriol was used to emit aerosols from the human mouth (the ratio of PBS to propanetriol in the solution was 23:2). In this experiment, a six-hole collision aerosol generator (ZR-C04) with an air pump was used to form the aerosol launching system. The air pump stably supplied clean air to the aerosol generator to ensure that the aerosol release rate, particle-size distribution, temperature, and humidity remained relatively stable.

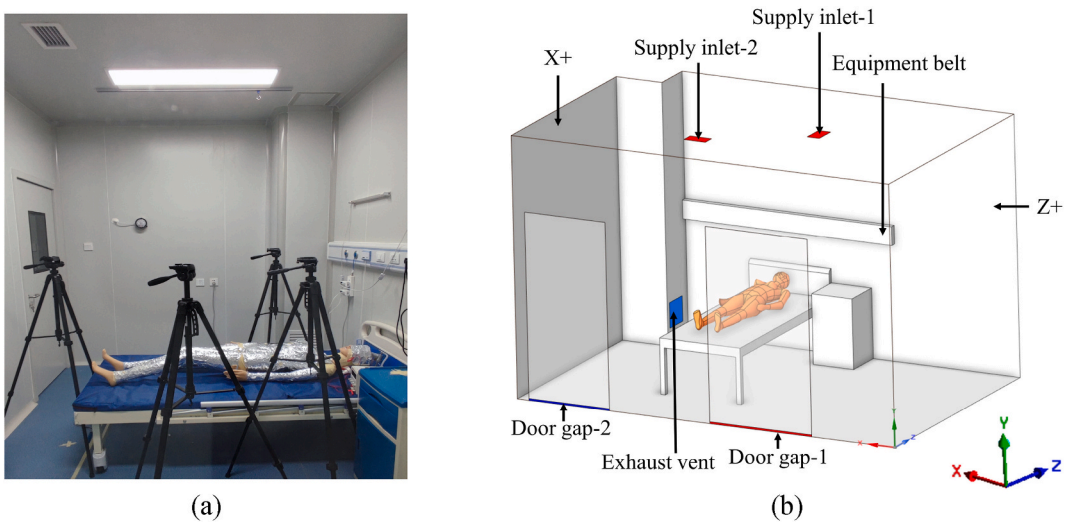

Fig. 1. A typical negative pressure isolation ward. (a) Aerosol experiment environment layout; (b) Numerical model layout.

One hour before the experiment, the air conditioning system of the ward was turned on to ensure that the environment in the room reached a relatively stable state. The airflow velocity was measured using an air velocity meter (TSI, model 9565, which has a measuring range of 0–30 m/s with an accuracy of ±3%). Eight air velocity measurement points were set up in the ward, and their respective positions are shown in Fig. 2(a). The aerosol sampling points used in the droplet aerosol experiments are shown in Fig. 2(b). Before releasing the aerosol, the background value of aerosol concentration at the four points was measured. The aerosol droplet is then released by the aerosol-generating system. After the aerosol was released for 600s, its concentration at each sampling point did not change significantly with time. Thus, the measurements for the concentration of droplet aerosols at the sampling point started 600s after the aerosol was released. Three parallel experiments were conducted to avoid errors. Three sets of data were obtained for each measurement point obtained from each experiment. The sampling flow was maintained at 1 L/min, and the data was collected for a total of 180s. Moreover, according to the recommendation of the *Requirements of environmental control for the hospital negative pressure isolation ward*, a constant air change rate (12 air changes per hour) was set in the ward. During the experiment, the ward had a relative humidity of 60% and temperature of 299.1 K.

2.3. Numerical simulation continuity phase and discrete phase

The indoor airflow was generally turbulent and could be simulated by two turbulence models: large eddy simulation (LES) and RANS (Reynolds Averaged Navier-Stokes) models. However, the computational cost required to apply the LES model for indoor flow-field simulations is too high [33]. Zhang et al. verified the stability of the RANS turbulence model in terms of accuracy, computational efficiency, and indoor environment modelling [34,35]. Therefore, the RNG k–ε turbulence model was used in this study to simulate the flow field environment inside the negative-pressure isolation ward. A standard wall function was used near the wall. The COUPLE algorithm was adopted to decouple pressure and velocity. The second-order upwind scheme was used to discretize the convection and diffusion convection terms in the governing equation. Simultaneously, the Boussinesq model is used to consider the buoyancy effect [10,36].

The primary governing equation for the continuous phase is expressed as follows [37]:

Energy equation,

$$\frac{\partial}{\partial x_i}(u_i(\rho e + p)) = \frac{\partial}{\partial x_i}\left(\lambda_{eff}\frac{\partial T}{\partial x_i} + u_j(\tau_{ij})_{eff}\right) + S_h \quad (1)$$

where x_i is the space coordinate component, u_i is the velocity in the

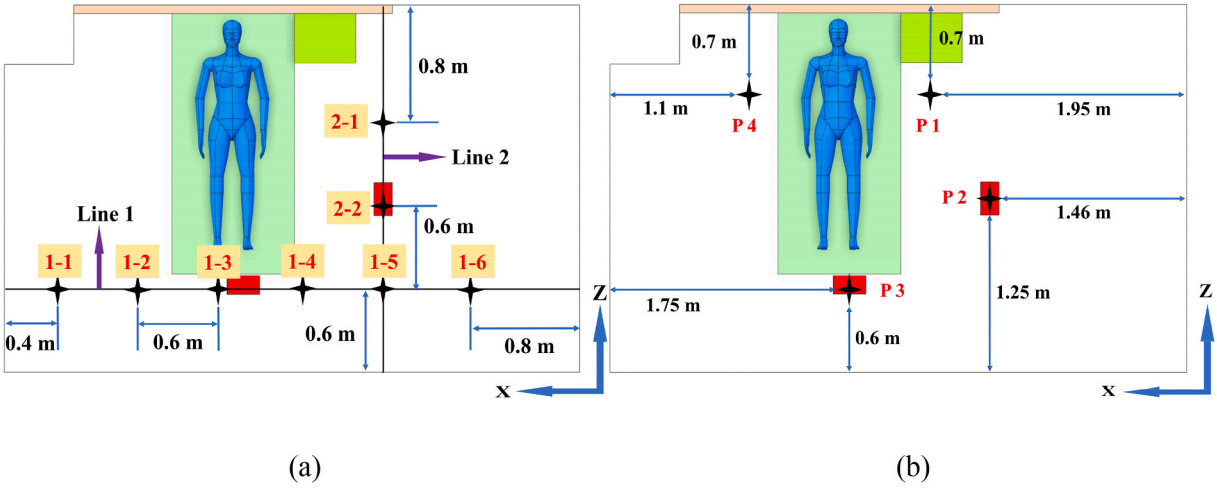

Fig. 2. The location of sampling points for (a) air velocity and (b) aerosol concentration.

$i$direction ($m \bullet s^{-1}$), ρ is the air density, e is the effective thermal conductivity, p is the pressure (Pa), λ_{eff} is the effective thermal conductivity ($W \bullet m^{-2} \bullet K^{-1}$), T is the temperature (K), u_i is the velocity in i direction ($m \bullet s^{-1}$), τ_{eff} is the effective dynamic viscosity, and S_h is the heat source ($N \bullet s^{-2}$).

Mass equation,

$$\frac{\partial(\rho u_i)}{\partial x_i} = 0 \tag{2}$$

where ρ is the air density, u_i is the velocity in the $i$direction ($m \bullet s^{-1}$), and x_i is the space coordinate component.

Momentum equation is

$$\frac{\partial(\rho u_i u_j)}{\partial x_j} = \frac{\partial}{\partial x_j}\left[\mu_{eff}\left(\frac{\partial u_i}{\partial x_j} + \frac{\partial u_j}{\partial x_i}\right) - \frac{2}{3}\mu_{eff}\frac{\partial u_k}{\partial x_k}\right] - \frac{\partial p}{\partial x_i} + \rho g_i + S_i$$

$$(i, j, k = 1, 2, 3 \text{ and } i \neq j) \tag{3}$$

where ρ is the air density, u_i is the velocity in the $i$direction ($m \bullet s^{-1}$), x_i is the space coordinate component, μ_{eff} is the effective dynamic viscosity ($Pa \bullet s$), ρ is the air density, e is the effective thermal conductivity, p is pressure (Pa), g_i is the gravitation acceleration in the $i$direction ($m \bullet s^{-2}$), S_i is the momentum sink ($N \bullet s^{-2}$), and i, j, k are the component values, which are equal to 1, 2 and 3, respectively.

The Lagrangian particle tracking model with a discrete random wander model was used to represent the vortex interaction of the discrete phase. To simplify the calculations, the following assumptions were made: the condensation of droplets was neglected, droplets were treated as spheres, and the effect of droplets on the airflow was not considered. The tracking of individual droplet trajectories followed Newton's second law, using the following control equation:

$$\frac{du_{pi}}{dt} = \sum F_i = F_{drag,i} + F_{g,i} + F_{a,i} \tag{4}$$

where u_{pi} is the droplet velocity in the i direction ($m \bullet s^{-1}$), t is time (s), ΣF_i is the sum of all external forces exerted on the droplet in the i direction ($m \bullet s^{-2}$), $F_{drag,i}$ is the drag force (N), $F_{g,i}$ is gravity (N), and $F_{a,i}$ is the additional force (N).

According to the results obtained from several studies [10,38,39], the additional forces on the droplet include the pressure gradient force, virtual mass force, Bassett force, Brownian force, and Saffman force. In our study, only Saffman and Brownian forces were considered. This is because these two forces played an important role in the droplet motion near the wall surface, whereas the other forces had a sufficiently small effect on the droplet motion [10,30].

Droplet aerosols consist of volatile and non-volatile components. The effect of non-volatile substances on droplet evaporation was ignored, and the droplet was viewed as a single-component substance. When a droplet evaporates in air, it reaches an equilibrium state and forms a droplet nucleus [40]. According to a study by Nicas, the evaporation ratio of a droplet was set to 92% [25]. The evaporation rate of the droplet depended mainly on the water vapor concentration gradient between the droplet surface and air environment. The droplet was controlled using the default evaporation control model of Fluent, and the controlling equation for the evaporation rate of the droplet is expressed as follows:

$$N_i = k_c\left(C_{i,s} - C_{i,sr}\right) \tag{5}$$

where N_i is the molar flux of the vapor ($kg \bullet molm^{-2} \bullet s^{-1}$), k_c is the mass transfer coefficient ($m \bullet s^{-1}$), $C_{i,s}$ is the vapor concentration at the droplet surface ($kg \bullet molm^{-3}$), and $C_{i,sr}$ is the vapor concentrations in the surrounding air ($kg \bullet molm^{-3}$).

3. Results and discussion

3.1. Validation of the numerical model

3.1.1. Grid independence validation

Fluent meshing was used to geometrically discretize the computational region and generate a tetrahedral unstructured mesh. The density and structure of the mesh are important and directly affect the accuracy of the subsequent flow field calculations [41,42]. Four different grids were used to ensure the accuracy of the continuous phase calculation. Two sample lines spanning the entire room at a horizontal height of 1.5 m are shown in Fig. 2(a). The velocity values of the two straight lines are extracted. The velocity distribution curves are shown in Fig. 3. As the number of grids increased, the four curves gradually approached each other. Among them, grids 2135231 had a large error, and the velocity fields were approximated in the remaining three grids. Considering the accuracy and calculation workload, a grid size of 2930761 was chosen for subsequent calculations. During this grid generation, finer meshes were used in locations with large velocity gradients, such as the mouth, supply inlets, exhaust vents, and door gaps. The mesh size of the mouth and the two-door gaps was 4 mm, which was smaller than the mesh around the human body by 20 mm. Simultaneously, the grid sizes of the supply inlets and exhaust vent were both set to 10 mm. Finally, the total number of grid elements was 2930761.

3.1.2. Validation of continuity phase

The flow field in the experimental environment was verified to ensure accuracy of the numerical calculation results. An air velocity meter (TSI, model 9565) was used to measure the velocity at eight measurement points, as shown in Fig. 2(a). Simultaneously, eight sampling points were numbered for easy statistical analysis. The sampling points were set on two lines (Line 1 and Line 2) across the room with a height of 1.5 m and a spacing of 0.6 m. A comparison of the simulated and experimentally measured values is shown in Fig. 3(a), (b). The discrepancy between the simulation and experimental results was small, which indicates that the grid setting, continuous phase model, and boundary condition setting in the numerical simulation were in line with the actual environment.

3.1.3. Validation of discrete phase

As shown in Fig. 4(a), in the droplet aerosol experiment, the droplet aerosol particle size distribution at the release source (histogram) and at four measuring points (point plot) were measured. After the aerosol was ejected from the mouth of the dummy model, it evaporated quickly to form a droplet nucleus. The evaporation ratio of droplet aerosols was close to 92% of our expectations. The droplet aerosol dimensionless concentrations measured in the artificial saliva experiment were compared with the results of the numerical calculations. Dimensionless concentration was defined as the ratio of the aerosol concentration at the sampling point to the mean value of the aerosol concentration at the four sampling points. The experimental measurements and simulation results of breathing are shown in Fig. 4(b). Considering the complexity of the sampling process, a certain degree of deviation is acceptable. Consequently, the concentration validation showed that the results of the discrete phase model were consistent with the experimental results, which ensured the accuracy of the subsequent numerical simulation.

3.2. Droplet diffusion under different respiratory behaviors

After droplet aerosols are released from the patient's mouth, they evaporate rapidly to form droplet nuclei. Thus, under the influence of gravity and buoyancy, the droplet aerosol was carried by the airflow of the air conditioning system to the ward. Few parts of the droplet aerosol were deposited on various surfaces, or they escaped from the exhaust vent and door gap, or the particles were still suspended in the ward. When the amount of suspended droplet aerosols in the space reached 1%

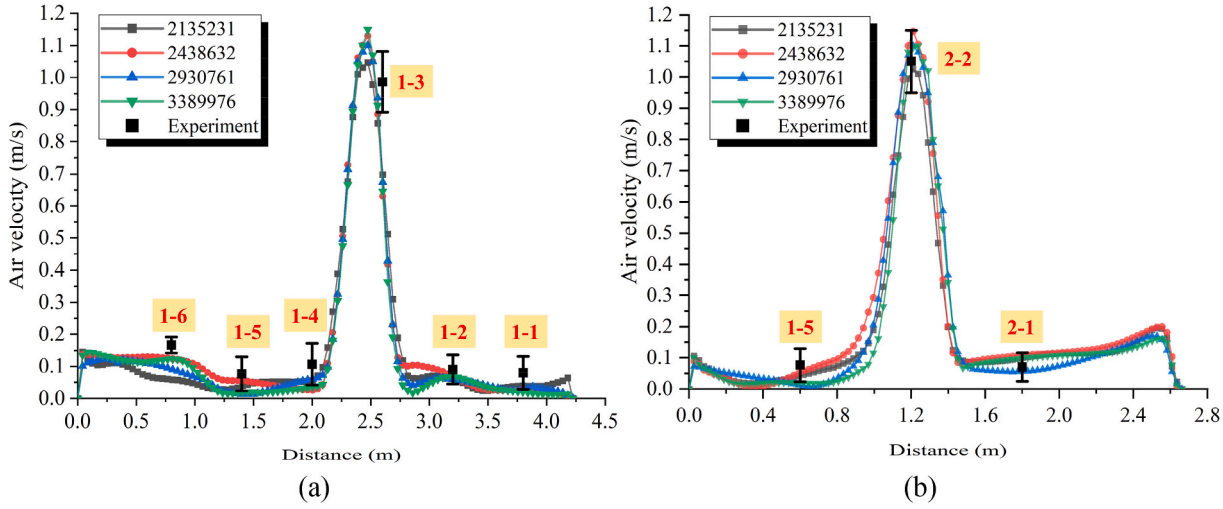

Fig. 3. The verification of grid independence and continuity phase. (a) Air velocity in Line 1 (b) Air velocity in Line 2.

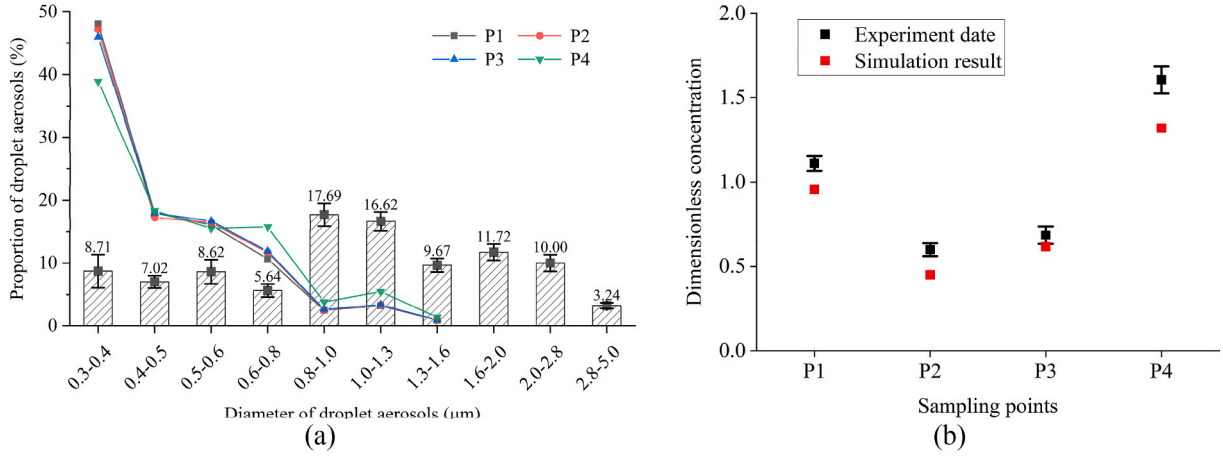

Fig. 4. The comparison of experimental and numerical results. (a) Particle size distribution of source and four measuring points; (b) Simulated and experimental values of droplet aerosols dimensionless concentrations.

of the total amount, the numerical calculation was stopped.

Fig. 5 depicts the proportion of droplets which were deposited, escaped, and suspended over time. The number of aerosol droplets released by the three respiratory behaviors differed. Therefore, the proportion, that is, the ratio of the number to the total number of droplet aerosols, was used to show the variation tendency of the droplet aerosols. Over 70% of the droplet aerosols were deposited on various surfaces of the ward. In the case of breathing, droplet aerosol injection was stopped at 600 s. After 160 s, the space suspension ratio decreased to 10%. It took longer to reduce the amount of space suspension for both speaking and coughing cases. However, the reduction in the suspension proportion per unit time was much higher than that in the case of breathing. This is because droplet aerosols generated by speaking and coughing have a faster diffusion rate.

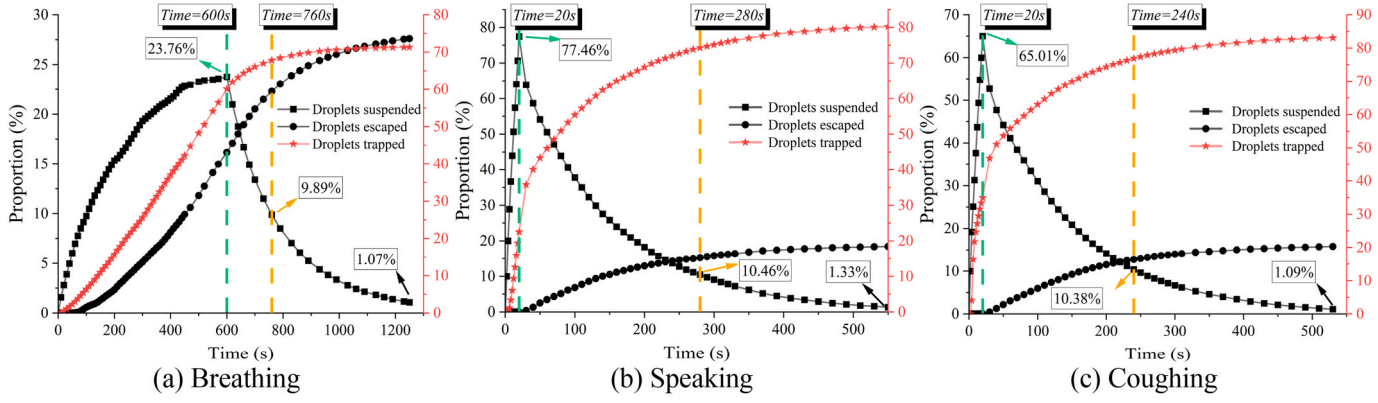

Fig. 5. The variation tendency of droplet aerosols proportion for three respiratory behaviors in the ward.

3.3. Spatial distribution of droplet aerosols in breathing zones of HCWs

HCWs exposed to high concentrations of aerosol droplets have a higher risk of infection. Tao et al. [43], used a sphere to count the number of aerosols in the breathing zone. The height of the center of this sphere was 1.6 m, and the diameter was 0.6 m. When treating patients, HCWs are more likely to stand on both sides of the bed. Meanwhile, the aerosol concentration under the air supply inlets was studied considering the dilution effect of fresh air on aerosols. Therefore, the locations of the four points shown in Fig. 2 (b) were used to determine aerosol concentrations at the respiratory height.

The statistics of the droplet aerosol concentration over time at the four points are shown in Fig. 6. With respect to the breathing and coughing cases, the aerosol concentration at point-3 was higher than that at the other points, whereas points 1 and 2 possessed lower aerosol concentrations. However, with respect to speaking, point-2 showed higher aerosol concentrations, while point-1 still possessed the lowest droplet aerosol concentration. As shown in Fig. 7, after the droplet aerosols left the mouth of the patient, they spread along the ceiling to supply inlet-2 and then flowed to supply inlet-1. The high concentration of aerosols was entrained by the supply air flow, resulting in a high concentration of aerosols below supply inlet-2. As shown in the enlarged view in Fig. 6, the airflow velocity produced by speaking and coughing was higher; therefore, droplet aerosols spread more quickly in the ward. In a short period of time, the droplet aerosols covered the entire ceiling and then spread in the ward following the supply airflow.

Although the air supplied by the system was clean, high aerosol concentrations were present around the supply inlets. These aerosols were carried by clean air, resulting in higher concentrations of droplet aerosols in the area around the main supply airflow. HCWs should avoid standing at point-2 when they spoke with the patient. HCWs at point-3 had a higher risk of infection when patients coughed frequently. In general, point-1 was located upwind of the droplet aerosol release source, and the droplet aerosol concentration was relatively low.

3.4. Deposition of droplet aerosols on various surfaces

Determining the main deposition locations of droplet aerosols is important for disinfection and sterilization inside wards. The distribution of droplet aerosol deposition inside the ward was obtained by simulating three exhalation methods. The deposition ratio is defined as the ratio of the total number of droplet aerosols deposited on each surface to the total number of droplet aerosols released. As shown in Fig. 8, the deposition ratio of the droplet aerosols on each wall of the room was compared when the number of aerosols in the space was approximately 1% of the total number of releases. It could be seen that the main deposition locations of droplet aerosols were on the ceiling (30.8%–37.6%), followed by the Z+ walls (12.7%–18.4%) and floor (9.1%–14.6%). However, the Z-walls and bed surfaces were deposited with relatively small amounts of aerosols, which was approximately 5.6%–6.8%.

On the ceiling, the rate of breathing deposition was 30.8%. After changing the exhalation mode, the deposition proportion of speaking increased to 35.0%, while the proportion of coughing increased to 37.6%. As shown in Fig. 9(a1-3), the number of particles in both the X- and Z-directions was distributed in a single peak. For the three working conditions, the deposition location was mainly concentrated directly above the aerosol release source, accounting for approximately 1/4 of the ceiling area. The main reasons were as follows: droplet aerosols were driven to the upper part of the space by the thermal plume formed to account for the heat dissipation of the human body, which has been demonstrated in existing studies [44,45], and part of the supply inlet-2 air supply blows along the human body towards the Z+ wall. This resulted in a large similarity in the main deposition locations in the three cases. To fully demonstrate the influence of these two factors on droplet aerosol transport, the flow field and temperature field contours at the human-mouth section are shown in Fig. 10. For breathing with a low air velocity, the droplet aerosols diffused to the Z+ wall side by the thermal plume and supply airflow. However, owing to the higher exhalation flow velocity generated by coughing and speaking, the diffusion of droplet aerosols was dominated by exhalation airflow. Therefore, the distribution of droplet aerosols from coughing and speaking on the ceiling is different from that of breathing.

The Z+ wall was second to the ceiling in terms of the droplet aerosol deposition. The distribution of the deposition locations is shown in Fig. 9 (b1-3), and a weak double-peak distribution of the particle number is displayed. Therefore, there should be two locations where deposition is relatively concentrated. One was on the wall above the release source, and the other was located in the lower left corner of the wall with relatively few deposits. When the respiratory speed is low, more droplet aerosols are transported to the Z+ wall by the supply airflow. In general, for all the three exhalation methods, a large amount of deposition occurred in the upper 1/3 of the Z+ wall. The deposition in the lower-left corner of the Z+ wall was caused by the airflow of supply inlet-1. The airflow from the top of the room reached the floor and spread downwards in all directions. At the same time, the air leakage from door gap-1 between the buffer room and the ward drives the droplet aerosols to migrate to the lower-left corner of the Z+ wall, as shown in Fig. 10(c).

Droplet aerosol deposition on the floor is shown in Fig. 9(c1-3). Two peaks of different sizes are observed in the deposition count statistics. Two densely deposited areas are observed on the floor. Deposition was evident under both air supply inlets; however, deposition under Supply

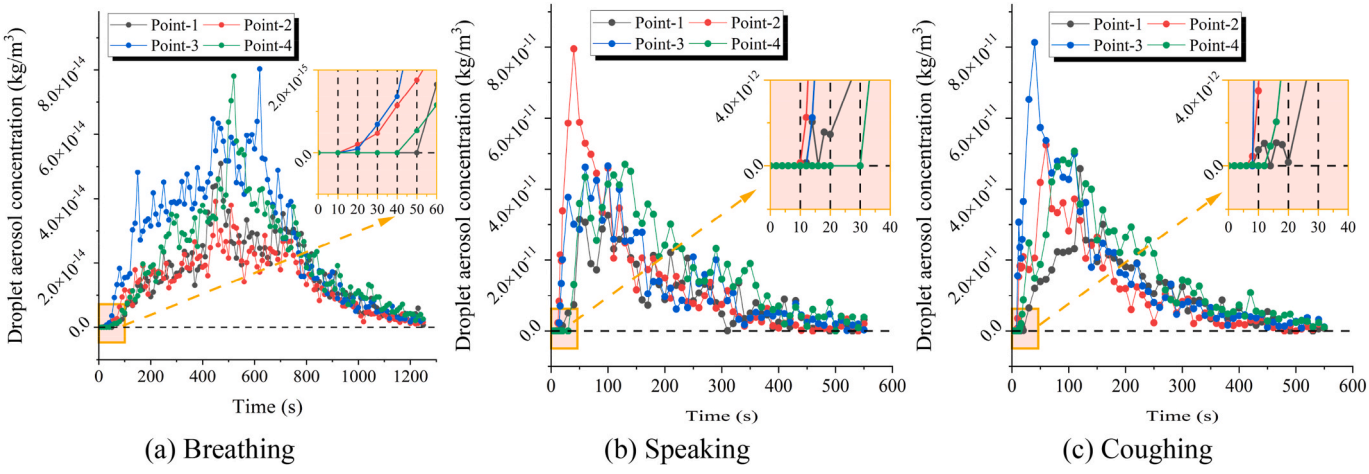

Fig. 6. The variation of droplet aerosols concentration for three respiratory behaviors at the four points.

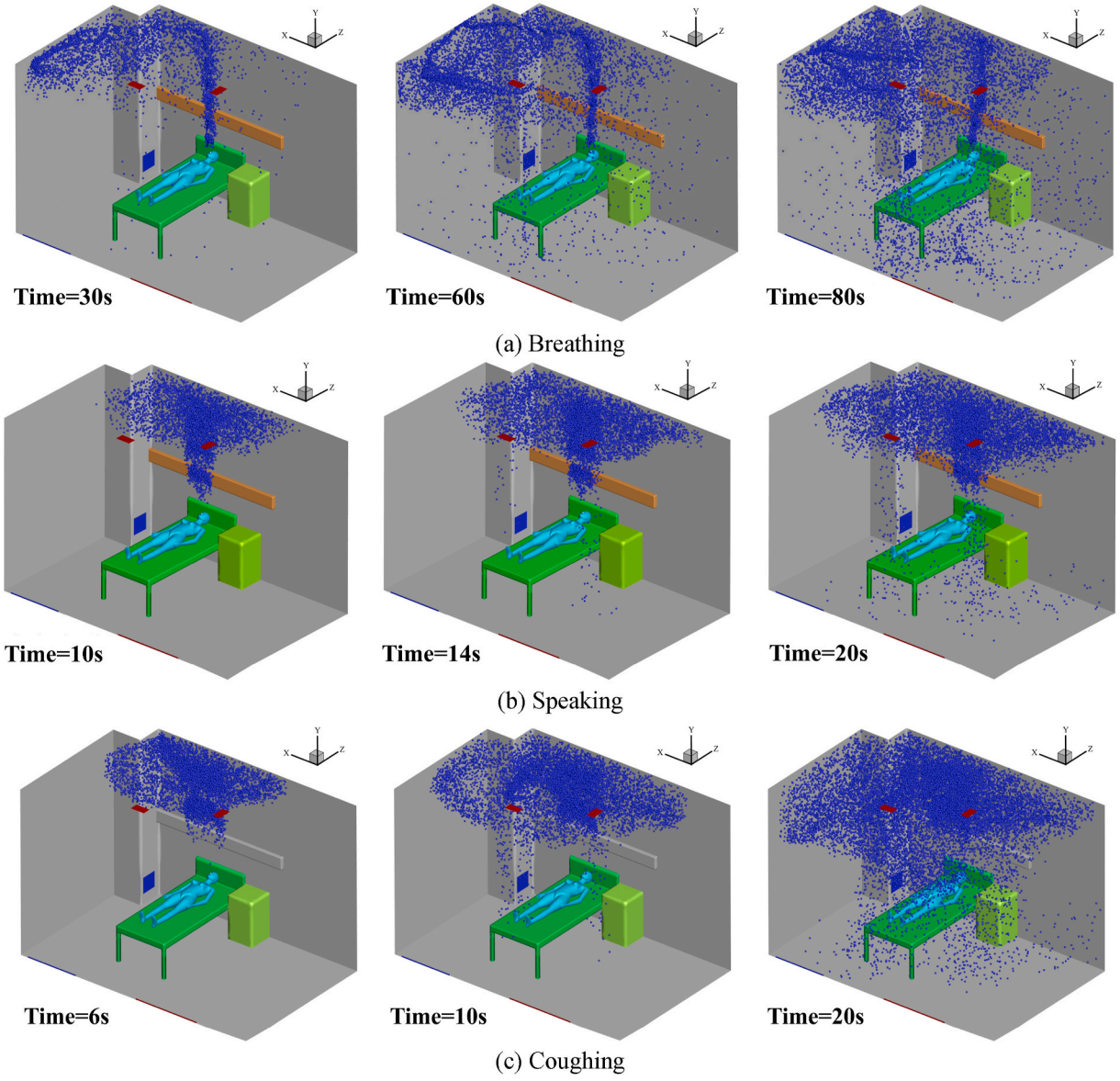

Fig. 7. Distribution of droplet aerosols at different time for three respiratory behaviors.

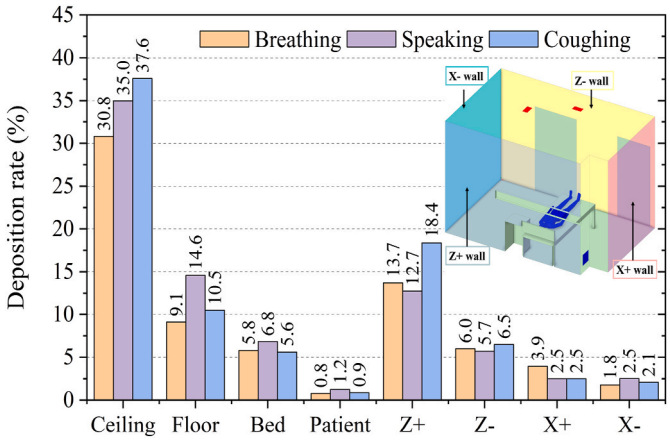

Fig. 8. Distribution of droplet aerosols deposition in the ward.

inlet-2 was denser. There was only a small amount of deposition in the 1.0–2.0 m region of the X-axis (Door gap-1). The reason for this was the air leakage from the buffer room. However, large quantity of air leaked to the bathroom through the 3.0–4.0 m region of the X-axis (Door gap-2), and a large amount of deposition occurred there. As the HCWs walked in these areas, the droplet aerosols that had been deposited were carried off the ground. Some studies have shown that sediment resuspension is an important source of airborne microorganisms [46]. Tao et al. used dynamic grid numerical calculations to verify that walking triggers the resuspension of massive droplet aerosols [43]. The resuspended aerosols were repeatedly transported by airflow [47]. Therefore, the ground below the air supply inlet was disinfected. Moreover, the frequency of HCWs activity during routine operations in these areas should be reduced.

3.5. *Limitations and future research*

In this study, all the patient was assumed be stationary. The relevant personnel movement makes the droplet distribution and spread more complicated. In future studies, droplet aerosol resuspension causing by personnel movement could be explored in detail. In addition, the design

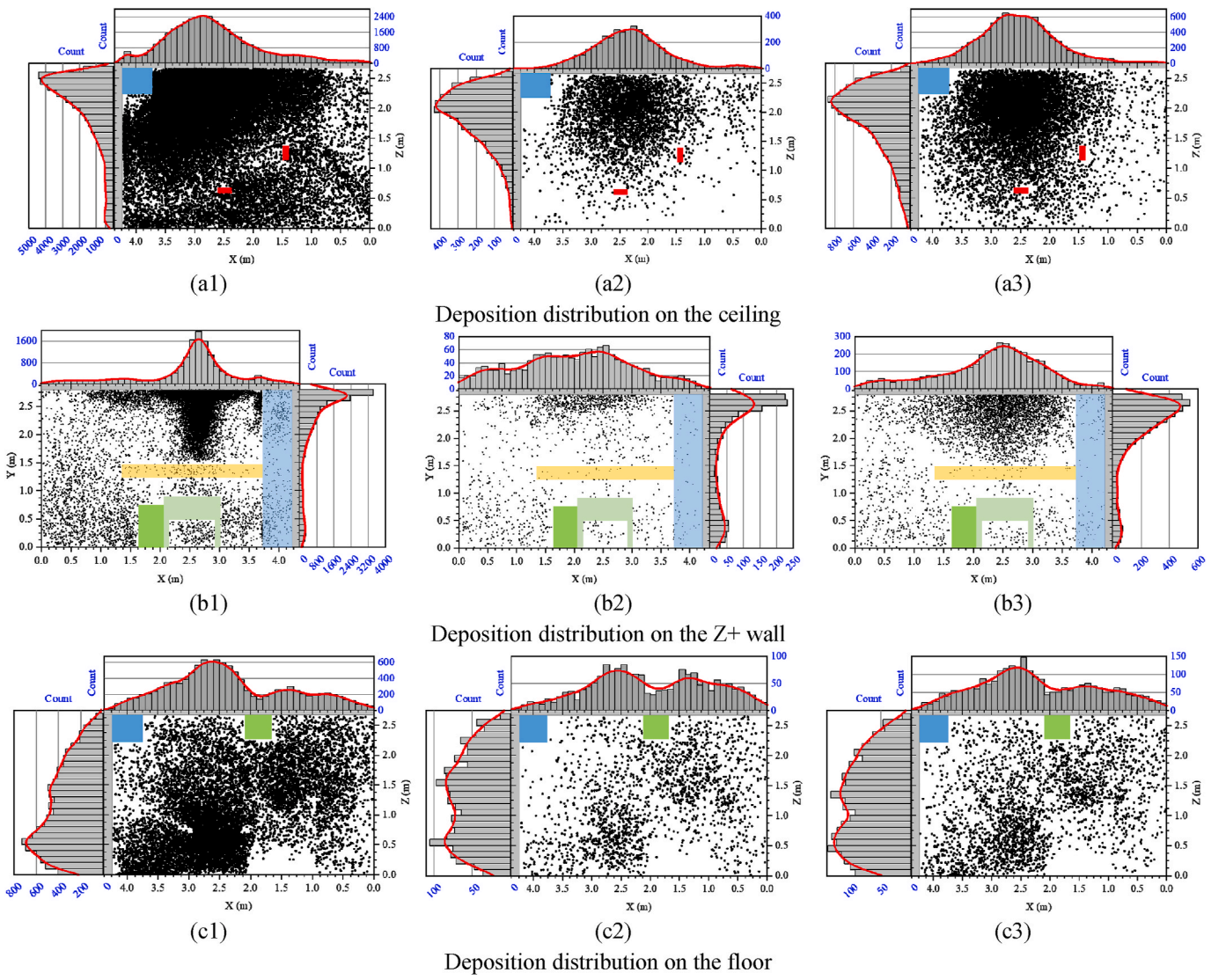

Fig. 9. Deposition distribution of droplet aerosols on the different surface under three respiratory behaviors: (a1, b1, c1) Breathing, (a2, b2, c2) Speaking, (a3, b3, c3) Coughing.

method of efficient ventilation for droplet aerosol exclusion could be investigated in depth.

4. Conclusion

In the negative-pressure isolation ward, HCWs are exposed to a high aerosol concentration environment, with potential risks of infection. The aim of our study was to improve the security of HCWs and reduce the risk of infection. Therefore, the distribution pattern of droplet aerosols was studied using both droplet aerosol experiments and numerical simulations. The deposition distribution of droplet aerosols generated by three respiratory behaviors (breathing, speaking, and coughing) in the ward was analyzed. Suggestions have also been proposed for the operation of negative-pressure isolation wards.

Some meaningful findings are addressed:

(1) Speaking and coughing could produce a higher velocity of expiratory airflow. Therefore, droplet aerosols spread faster than those produced by breathing. Droplet aerosols generated by coughing and speaking can be removed and deposited more rapidly.

(2) Approximately 10% of the droplet aerosols were deposited on the floor, with the majority deposited under the supply inlets. Frequent movement of personnel in this area could cause resuspension of deposited aerosols. Simultaneously, more droplet aerosols might be deposited on the surfaces of HCWs when they are under the supply inlets.

(3) In our study, this airflow organization could control the lower aerosol concentrations in the right half of the ward. However, the concentration of droplet aerosols in the area below the air supply inlets might be higher, leading to a higher risk of infection for HCWs.

CRediT authorship contribution statement

Yongxin Wang: Writing – review & editing, Writing – original draft, Software, Project administration, Methodology, Formal analysis, Data curation, Conceptualization. **Zhijian Liu:** Writing – review & editing, Project administration, Funding acquisition, Conceptualization. **Haiyang Liu:** Writing – review & editing, Writing – original draft, Software, Formal analysis. **Minnan Wu:** Writing – review & editing, Software, Formal analysis. **Junzhou He:** Writing – review & editing, Methodology. **Guoqing Cao:** Software, Methodology.

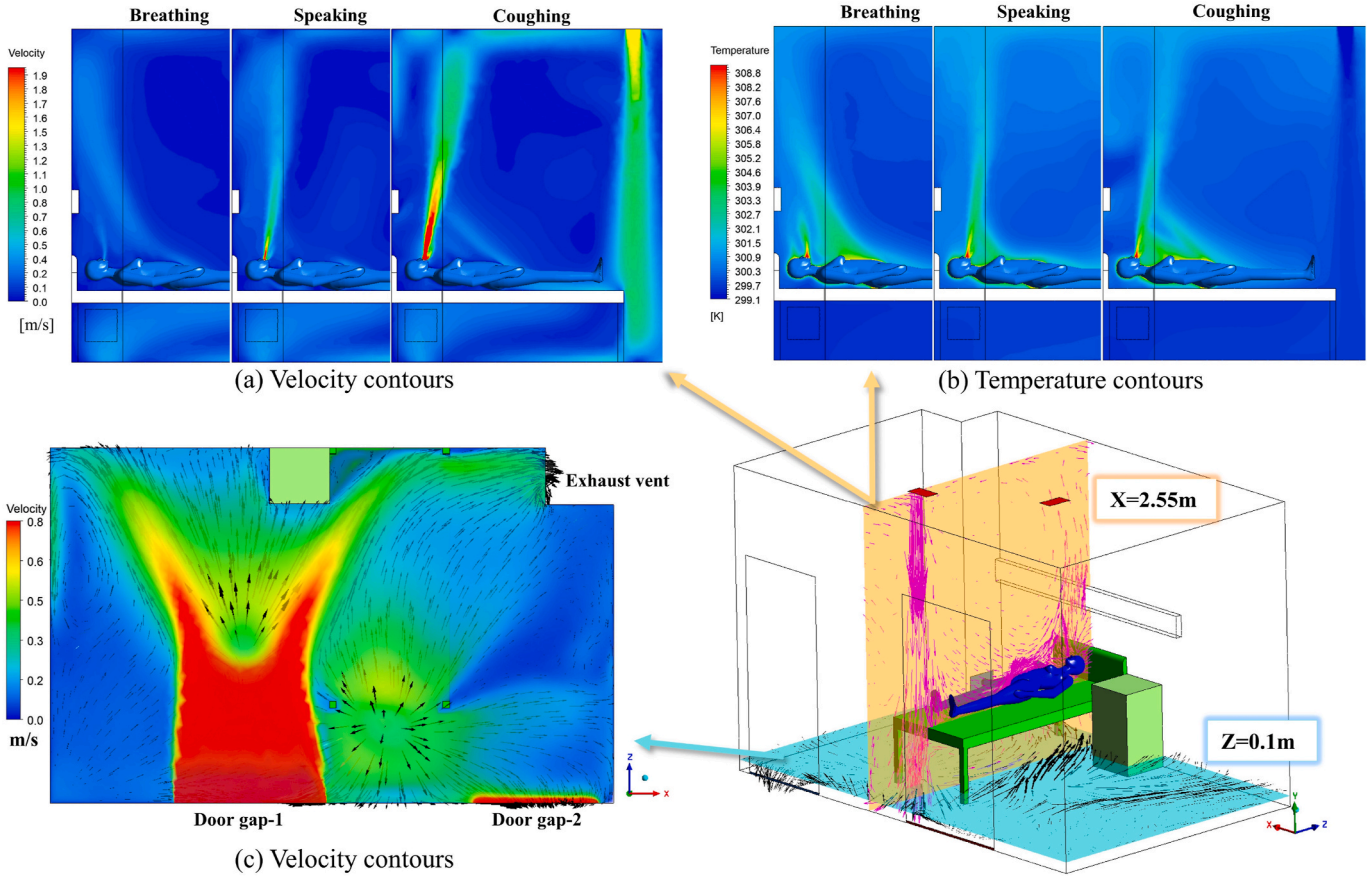

Fig. 10. The contours at the selected planes: (a) velocity contours at the plane of X = 2.55 m, (b) temperature contours at the plane of X = 2.55 m and (c) velocity contours and vector at the plane of Z = 0.1 m.

Declaration of competing interest

The authors declare that they have no known competing financial interests or personal relationships that could have appeared to influence the work reported in this paper.

Acknowledgement

This work was supported by the National Key R&D Program of China (2021YFF0604000), the National Natural Science Foundation of China (Nos. 42122058 and 41977368), Natural Science Foundation of Hebei Province (No. E2021502046), and Fundamental Research Funds for the Central Universities (Nos. 2021MS075 and 2020YJ007).

References

[1] WHO Director-General's opening remarks at the media briefing on COVID-19-1. https://www.who.int/director-general/speeches/detail, 2022.
[2] J.A. Cepeda, T. Whitehouse, B. Cooper, J. Hails, K. Jones, F. Kwaku, L. Taylor, S. Hayman, B. Cookson, S. Show, C. Kibbler, M. Singer, G. Bellingan, A.P.R. Wilson, Isolation of patients in single rooms or cohorts to reduce spread of MRSA in intensive-care units: prospective two-centre study, Lancet 365 (9456) (2005) 295–304.
[3] S.L. Miller, D. Mukherjee, J. Wilson, N. Clements, C. Steiner, Implementing a negative pressure isolation space within a skilled nursing facility to control SARS-CoV-2 transmission, Am. J. Infect. Control 49 (4) (2021) 438–446.
[4] J.K. Lee, H.W. Jeong, Rapid expansion of temporary, reliable airborne -infection isolation rooms with negative air machines for critical COVID-19 patients, Am. J. Infect. Control 48 (7) (2020) 822–824.
[5] C.C. Wang, K.A. Prather, J. Sznitman, J.L. Jimenez, S.S. Lakdawala, Z. Tufekci, L. C. Marr, Airborne transmission of respiratory viruses, Science 373 (6558) (2021).
[6] L. Morawska, J. Cao, Airborne transmission of SARS-CoV-2: the world should face the reality, Environ. Int. 139 (2020).
[7] I.T.S. Yu, Y.G. Li, T.W. Wong, W. Tam, A.T. Chan, J.H.W. Lee, D.Y.C. Leung, T. Ho, Evidence of airborne transmission of the severe acute respiratory syndrome virus, N. Engl. J. Med. 350 (17) (2004) 1731–1739.
[8] A. Jurelionis, L. Gagytė, T. Prasauskas, D. Čiužas, E. Krugly, L. Šeduikytė, D. Martuzevičius, The impact of the air distribution method in ventilated rooms on the aerosol particle dispersion and removal: the experimental approach, Energy Build. 86 (2015) 305–313.
[9] Y. Yin, J.K. Gupta, X. Zhang, J. Liu, Q. Chen, Distributions of respiratory contaminants from a patient with different postures and exhaling modes in a single-bed inpatient room, Build. Environ. 46 (1) (2011) 75–81.
[10] B. Zhao, Y. Zhang, X.T. Li, X.D. Yang, D.T. Huang, Comparison of indoor aerosol particle concentration and deposition in different ventilated rooms by numerical method, Build. Environ. 39 (1) (2004) 1–8.
[11] I. Olmedo, P.V. Nielsen, M.R. de Adana, R.L. Jensen, P. Grzelecki, Distribution of exhaled contaminants and personal exposure in a room using three different air distribution strategies, Indoor Air 22 (1) (2012) 64–76.
[12] S.B. Kwon, J. Park, J. Jang, Y. Cho, D.S. Park, C. Kim, G.N. Bae, A. Jang, Study on the initial velocity distribution of exhaled air from coughing and speaking, Chemosphere 87 (11) (2012) 1260–1264.
[13] P. Fabian, J. Brain, E.A. Houseman, J. Gern, D.K. Milton, Origin of exhaled breath particles from healthy and human rhinovirus-infected subjects, J. Aerosol Med. Pulm. Drug Deliv. 24 (3) (2011) 137–147.
[14] J.K. Gupta, C.H. Lin, Q. Chen, Flow dynamics and characterization of a cough, Indoor Air 19 (6) (2009) 517–525.
[15] C.Y.H. Chao, M.P. Wan, L. Morawska, G.R. Johnson, Z.D. Ristovski, M. Hargreaves, K. Mengersen, S. Corbett, Y. Li, X. Xie, D. Katoshevski, Characterization of expiration air jets and droplet size distributions immediately at the mouth opening, J. Aerosol Sci. 40 (2) (2009) 122–133.
[16] S. Yang, G.W.M. Lee, C.-M. Chen, C.-C. Wu, K.-P. Yu, The size and concentration of droplets generated by coughing in human subjects, Journal of Aerosol Medicine-Deposition Clearance and Effects in the Lung 20 (4) (2007) 484–494.
[17] J.P. Duguid, The size and the duration of air-carriage of respiratory droplets and droplet-nuclei, J. Hyg. 44 (6) (1946) 471–479.
[18] L. Morawska, J. Allen, W. Bahnfleth, P.M. Bluyssen, A. Boerstra, G. Buonanno, J. Cao, S.J. Dancer, A. Floto, F. Franchimon, T. Greenhalgh, C. Haworth, J. Hogeling, C. Isaxon, J.L. Jimenez, J. Kurnitski, Y. Li, M. Loomans, G. Marks, L. C. Marr, L. Mazzarella, A.K. Melikov, S. Miller, D.K. Milton, W. Nazaroff, P. V. Nielsen, C. Noakes, J. Peccia, K. Prather, X. Querol, C. Sekhar, O. Seppanen, S.-i. Tanabe, J.W. Tang, R. Tellier, K.W. Tham, P. Wargocki, A. Wierzbicka, M. Yao,

A paradigm shift to combat indoor respiratory infection Building ventilation systems must get much better, Science 372 (6543) (2021) 689.
[19] R. Zhang, Y. Li, A.L. Zhang, Y. Wang, M.J. Molina, Identifying airborne transmission as the dominant route for the spread of COVID-19, Proc. Natl. Acad. Sci. U.S.A. 117 (26) (2020) 14857–14863.
[20] R. Tellier, Y. Li, B.J. Cowling, J.W. Tang, Recognition of aerosol transmission of infectious agents: a commentary, BMC Infect. Dis. 19 (2019).
[21] L.D. Knibbs, L. Morawska, S.C. Bell, P. Grzybowski, Room ventilation and the risk of airborne infection transmission in 3 health care settings within a large teaching hospital, Am. J. Infect. Control 39 (10) (2011) 866–872.
[22] P. Kalliomaki, P. Saarinen, J.W. Tang, H. Koskela, Airflow patterns through single hinged and sliding doors in hospital isolation rooms - effect of ventilation, flow differential and passage, Build. Environ. 107 (2016) 154–168.
[23] Y. Zhou, S. Ji, Experimental and numerical study on the transport of droplet aerosols generated by occupants in a fever clinic, Build. Environ. 187 (2021).
[24] C.Y.H. Chao, M.P. Wan, A study of the dispersion of expiratory aerosols in unidirectional downward and ceiling-return type airflows using a multiphase approach, Indoor Air 16 (4) (2006) 296–312.
[25] M. Nicas, W.W. Nazaroff, A. Hubbard, Toward understanding the risk of secondary airborne infection: emission of respirable pathogens, J. Occup. Environ. Hyg. 2 (3) (2005) 143–154.
[26] T. Nasserie, M. Hittle, S.N. Goodman, Assessment of the frequency and variety of persistent symptoms among patients with COVID-19 A systematic review, JAMA Netw. Open 4 (5) (2021).
[27] T. Struyf, J.J. Deeks, J. Dinnes, Y. Takwoingi, C. Davenport, M.M.G. Leeflang, R. Spijker, L. Hooft, D. Emperador, S. Dittrich, J. Domen, S.R.A. Horn, A. Van den Bruel, C.-D.T.A. Cochrane, Signs and symptoms to determine if a patient presenting in primary care or hospital outpatient settings has COVID-19 disease, Cochrane Database Syst. Rev. 7 (2020).
[28] C. Menni, A.M. Valdes, L. Polidori, M. Antonelli, S. Penamakuri, A. Nogal, P. Louca, A. May, J.C. Figueiredo, C. Hu, E. Molteni, L. Canas, M.F. Österdahl, M. Modat, C. H. Sudre, B. Fox, A. Hammers, J. Wolf, J. Capdevila, A.T. Chan, S.P. David, C. J. Steves, S. Ourselin, T.D. Spector, Symptom prevalence, duration, and risk of hospital admission in individuals infected with SARS-CoV-2 during periods of omicron and delta variant dominance: a prospective observational study from the ZOE COVID Study, Lancet 399 (10335) (2022) 1618–1624.
[29] L. Morawska, G.R. Johnson, Z.D. Ristovski, M. Hargreaves, K. Mengersen, S. Corbett, C.Y.H. Chao, Y. Li, D. Katoshevski, Size distribution and sites of origin of droplets expelled from the human respiratory tract during expiratory activities, J. Aerosol Sci. 40 (3) (2009) 256–269.
[30] X. Yang, C. Ou, H. Yang, L. Liu, T. Song, M. Kang, H. Lin, J. Hang, Transmission of pathogen-laden expiratory droplets in a coach bus, J. Hazard Mater. 397 (2020) 122609.
[31] J.J. Wei, Y.G. Li, Enhanced spread of expiratory droplets by turbulence in a cough jet, Build. Environ. 93 (2015) 86–96.
[32] W.T. Leung, G.N. Sze-To, C.Y.H. Chao, S.C.T. Yu, J.K.C. Kwan, Study on the interzonal migration of airborne infectious particles in an isolation ward using benign bacteria, Indoor Air 23 (2) (2013) 148–161.
[33] J.I. Choi, J.R. Edwards, Large-eddy simulation of human-induced contaminant transport in room compartments, Indoor Air 22 (1) (2012) 77–87.
[34] Z. Zhang, Z. Zhai, W. Zhang, Q. Chen, Evaluation of various turbulence models in predicting airflow and turbulence in enclosed environments by CFD: Part 2-comparison with experimental data from literature, HVAC R Res. 13 (6) (2007) 871–886.
[35] Z. Zhang, X. Chen, S. Mazumdar, T. Zhang, Q. Chen, Experimental and numerical investigation of airflow and contaminant transport in an airliner cabin mockup, Build. Environ. 44 (1) (2009) 85–94.
[36] B.E. Launder, D.B. Spalding, The numerical computation of turbulence flows, Computing Methods Applied Mechanical Engineering (3) (1974) 269.
[37] A.F.20. 1, Theory Guide, Ansys Inc., 2020.
[38] L. Zhang, Y. Li, Dispersion of coughed droplets in a fully-occupied high-speed rail cabin, Build. Environ. 47 (2012) 58–66.
[39] J.K. Gupta, C.-H. Lin, Q. Chen, Characterizing exhaled airflow from breathing and talking, Indoor Air 20 (1) (2010) 31–39.
[40] L. Liu, J. Wei, Y. Li, A. Ooi, Evaporation and dispersion of respiratory droplets from coughing, Indoor Air 27 (1) (2017) 179–190.
[41] Y. Li, X. Huang, I.T.S. Yu, T.W. Wong, H. Qian, Role of air distribution in SARS transmission during the largest nosocomial outbreak in Hong Kong, Indoor Air 15 (2) (2005) 83–95.
[42] A.F. Nielsen Pv, H.B. Awbi, L. Davidson, A. Schälin, CFD in Ventilation Design: a New REHVA Guide Book, Aalborg University, 2009.
[43] Y. Tao, K. Inthavong, J.Y. Tu, Dynamic meshing modelling for particle resuspension caused by swinging manikin motion, Build. Environ. 123 (2017) 529–542.
[44] Y. Yan, X. Li, J. Tu, Thermal effect of human body on cough droplets evaporation and dispersion in an enclosed space, Build. Environ. 148 (2019) 96–106.
[45] M. Salmanzadeh, G. Zahedi, G. Ahmadi, D.R. Marr, M. Glauser, Computational modeling of effects of thermal plume adjacent to the body on the indoor airflow and particle transport, J. Aerosol Sci. 53 (2012) 29–39.
[46] A.J. Prussin, L.C. Marr, Sources of airborne microorganisms in the built environment, Microbiome 3 (2015).
[47] I. Goldasteh, Y. Tian, G. Ahmadi, A.R. Ferro, Human induced flow field and resultant particle resuspension and transport during gait cycle, Build. Environ. 77 (2014) 101–109.